Geophysical Prospecting **39**, 757–781, 1991

TUNNELLING AND THE GENERALIZED RAY METHOD IN PIECEWISE HOMOGENEOUS MEDIA[1]

GUY G. DRIJKONINGEN[2]

ABSTRACT

DRIJKONINGEN, G.G. 1991. Tunnelling and the generalized ray method in piecewise homogeneous media. *Geophysical Prospecting* **39**, 757–781.

The contributions of the tunnelled constituents to a seismic wave are analysed in two different configurations pertaining to homogeneous acoustic media: a thin high-velocity layer, present in a plane-layered configuration, and a thin layer in media separated by dipping interfaces. The generalized ray method in the far-field is used to determine them. We expand around the relevant ray parameters in order to determine the characteristics of the tunnelling ray and find that the most important feature of this type of ray is a phase (in terms of asymptotic ray theory) which has a real and an imaginary part. Numerical results illustrate this.

INTRODUCTION

Tunnelling is the physical process which occurs when a plane wave impinges at an angle greater than the critical angle on a scattering object, in this case plane interfaces. The contribution from the resultant constituents is often neglected either because, due to the physical configuration, its occurrence is not suspected or because it can be shown mathematically to be negligible. However, in seismology and seismic exploration many cases exist where tunnelling can be important. This has been shown by, among others, Fuchs and Schulz (1976) with investigations into the lower crust; by Hron and Mikhailenko (1981) with the so-called S* wave; by Daley and Hron (1983); and by Stephen and Bolmer (1985), who give an example of the source being near to an interface using the 'direct-wave root'. In the published examples the analysis used to investigate the tunnelling phenomenon is rather awkward, since the effect of tunnelling is not obvious in the numerical schemes. In Drijkoningen and Chapman (1988) the characteristics of tunnelling were revealed by

[1] Received June 1990, revision accepted March 1991.

[2] Bullard Laboratories, University of Cambridge. Present address: Faculty of Mining and Petroleum Engineering, Technical University Delft, P.O. Box 5028, 2600 GA Delft, The Netherlands.

investigating a canonical problem to which the Cagniard–De Hoop method (Cagniard 1939, 1962; De Hoop 1960) was applied. A different analysis can be found in Abramovici, Le and Kanasewich (1989). Here, we first analyse a thin high-velocity layer, a situation often occurring in practice.

The second configuration considered here is a thin layer, wedging out in an environment of layers separated by dipping interfaces. Dipping interfaces have been studied before by Hong and Helmberger (1977, 1978), using the exact solution of the wedge problem (Hudson 1963). Their analysis was approximate, but recently it has been discovered that an exact Cagniard–de Hoop analysis can be applied to the wedge (Pao, Ziegler and Wang 1989). However, here we shall use the far-field approximation which simplifies the analysis of configurations with many interfaces.

The order of the steps for investigating the stated ray problem is standard. We begin by solving the wave equation itself using the asymptotic theory, as applied by Chapman and Drummond (1982) to seismological problems, but we do not need to consider caustics. The solution obtained in this way is general enough to deal with our configurations. The next step is to obtain the space–time domain response, i.e. the synthetic seismogram, since we have made use of some integral transforms (Fourier transforms) in the first step. We shall use a modification of the Cagniard–De Hoop method which involves the high-frequency approximation and is commonly called the generalized ray method. Since we have introduced an approximation, we can now investigate less restricted kinds of configurations. The generalized ray method was chosen firstly, because it can be used to investigate tunnelling, and secondly, because we also wanted to see the results in laterally inhomogeneous media.

In order to appreciate the characteristics of the tunnelling ray, we expand the (general) response about the relevant ray parameters. These expansions give us more physical insight into the phenomenon which is important for interpretation. They show whether we actually see what we expect to see.

Analytical Considerations

We discuss the basic notion of the theory as given in Chapman and Drummond (1982). We begin with the inhomogeneous wave equation for the line source,

$$\frac{\partial^2 P}{\partial x^2} + \frac{\partial^2 P}{\partial z^2} - \frac{1}{\alpha^2}\frac{\partial^2 P}{\partial t^2} = -\delta(t, x, z), \tag{1}$$

where P denotes the pressure, x and z are the horizontal and vertical coordinates respectively, t denotes time and α is the wave speed. The inhomogeneous term on the right-hand side of the equation is due to the source which in our case is taken to be the Dirac pulse. Initially we omit this term and only in the final stages of the solution include it by matching the wavefield at the source and receiver.

Let us define a temporal Fourier transformation with respect to time as

$$\hat{P}(\omega) = \int_{-\infty}^{\infty} P(t) \exp(i\omega t)\, dt. \tag{2}$$

Applying this transformation to (1) without the source term yields the Helmholtz' equation

$$\nabla^2 \hat{P} + \frac{\omega^2}{\alpha^2(\mathbf{x})} \hat{P} = 0, \tag{3}$$

where ∇ denotes the gradient operator. We now look for an asymptotic solution to this form of the wave equation, which is a well-known procedure in asymptotic ray theory (ART). We look for solutions of the form

$$\hat{P} \sim \sum_{n=0}^{\infty} \frac{A^{(n)}(\mathbf{x})}{(-\mathrm{i}\omega)^n} \exp(\mathrm{i}\omega T(\mathbf{x})), \tag{4}$$

which we substitute into (3) and equate powers of ω. The resulting equations enable us to solve for T and $A^{(n)}$ (see e.g. Červený and Ravindra 1971; Chapman and Drummond 1982). The phase T is resolved by solving the equation for the coefficient ω^2. Defining the ray direction $\mathbf{s}$ by $\mathbf{s} = \nabla T$, this equation then gives us the solution

$$\frac{d}{dv} \mathbf{x} = \mathbf{s}, \tag{5}$$

$$\frac{d}{dv} \mathbf{s} = (\alpha^{-1}) \nabla (\alpha^{-1}), \tag{6}$$

where v is the ray coordinate, according to the definition of Chapman and Drummond (1982). Although the solution is obtained for continuously varying media, only the equations for homogeneous regions are needed here. In such regions the gradient term $\nabla(\alpha^{-1})$ is zero and the rays are straight lines in space. This characteristic will be used below for deriving formulae suitable for configurations with dipping interfaces. The term $A^{(0)}$ is resolved by solving the equation for the coefficient ω^1. The solution is of the form:

$$A^{(0)}(\mathbf{x}) = A^{(0)}(\mathbf{x}_0) \left| \frac{\partial \mathbf{x}}{\partial \mathbf{x}_0} \right|_v^{-1/2}, \tag{7}$$

where the term $| \partial \mathbf{x} / \partial \mathbf{x}_0 |_v^{-1/2}$ represents the geometric spreading factor.

We now apply a Fourier transformation with respect to the horizontal coordinate to the high-frequency solution obtained above,

$$\tilde{P}^{(0)}(\omega, p) = \int_{-\infty}^{\infty} A^{(0)} \exp(\mathrm{i}\omega(T - px)) \, \mathrm{d}x. \tag{8}$$

In this transformation p can be related to the (local) horizontal component of the ray vector. We evaluate this integral assuming the main contribution to the integral occurs where the phase is stationary. Designating the values of x at which the phase is stationary as $X(p)$, we obtain

$$\tilde{P}^{(0)}(\omega, p) \simeq \left(\frac{2\pi}{\omega} \right)^{1/2} A^{(0)}(X(p)) \left| \frac{\partial p}{\partial x} \right|_{x = X(p)}^{-1/2} \exp(\mathrm{i}\omega\tau) \exp(\mathrm{i}\pi/4), \tag{9}$$

where

$$\tau = T(X(p)) - pX(p). \tag{10}$$

The above result is the desired asymptotic transform-domain expression corresponding to the zeroth-order term in the ART expansion. This derivation differs from previous methods, in which the transform-domain expression was derived by simply replacing $\partial/\partial x$ by $i\omega p$ in the wave equation. It is now obvious that this cannot always be done 'for all x'. It is also clear from the above expressions that the ray tracing is necessary in order to obtain the response. This fact will be used when discussing tunnelling in media with dipping interfaces. In order to complete the solution in the frequency–slowness domain, we match the wavefield to the source and receiver. Then finally, to obtain the synthetic seismogram, we must invert to the space–time domain. As the solution is in the frequency–slowness domain we have several methods at our disposal, but since we are interested in the physical features of the tunnelling phenomenon we choose a method where we can perform the inverse temporal Fourier transform analytically. Furthermore, we want a method which can model tunnelling and therefore the generalized ray method (Helmberger 1968), based on the Cagniard–De Hoop method (Cagniard 1939, 1962; De Hoop 1960), is suitable.

In order to illustrate the generalized ray method we shall discuss it briefly using Heyman and Felsen's (1984, 1987) formulation. We apply the method to the expression which includes matching of the wavefield at the source and receiver,

$$\tilde{P}(\omega, p) = \frac{\mathrm{i}}{2\omega} A \exp(\mathrm{i}\omega\tau). \tag{11}$$

The space–time domain equivalent is given by

$$P(t, \mathbf{x}) = \frac{1}{4\pi^2} \int_{-\infty}^{\infty}\int_{-\infty}^{\infty} \frac{\mathrm{i}}{2\omega} A \exp\{-\mathrm{i}\omega(t - px - \tau)\} |\omega| \, \mathrm{d}p \, \mathrm{d}\omega. \tag{12}$$

We now change the order of integration and integrate over the frequencies, separating the positive and negative frequencies. The result (Heyman and Felsen) is

$$P(t, \mathbf{x}) = \frac{1}{8\pi^2}\left(\int_{-\infty+\mathrm{i}\varepsilon}^{\infty-\mathrm{i}\varepsilon} \frac{A}{t-\theta}\,\mathrm{d}p + \int_{-\infty-\mathrm{i}\varepsilon}^{\infty+\mathrm{i}\varepsilon} \frac{A}{t-\theta}\,\mathrm{d}p\right), \tag{13}$$

where

$$\theta = px + \tau = T(X(p)) + p(x - X(p)) \tag{14}$$

and ε is a small quantity to denote that the paths of integration run infinitesimally above or below the real p-axis.

Equation (14), $\theta = \theta(p)$ has complex solutions in p for times greater than the geometrical arrival time (T_s). This contour, $p = p(\theta)$, has been called the Cagniard contour. Figure 1a shows the situation for the first integral in (13). We deform the original contour into the complex plane with an arc at infinity which does not contribute. The contribution due to the path of integration along the solutions

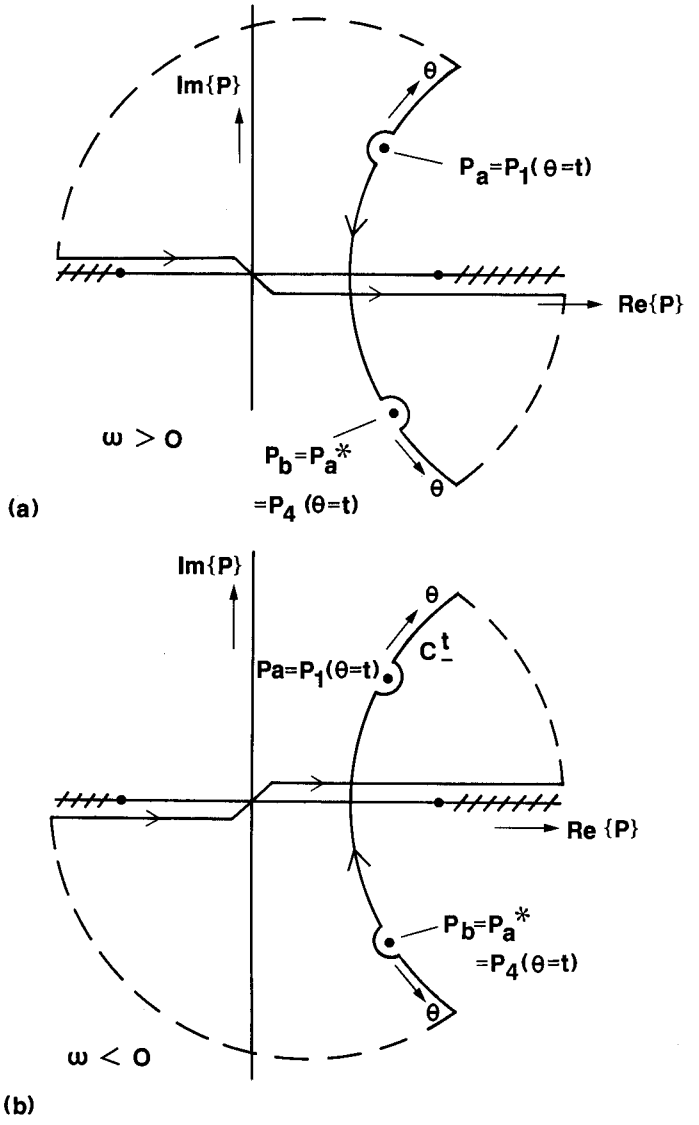

FIG. 1. Solutions p of contour $t = \theta$ in complex p domain. Original path of integration along real p axis deformed to path C^t_+ (dashed) in (a) and to C^t_- in (b). Poles denoted by circles; s_1 are solutions in first quadrant, s_4 in fourth.

$p = p(\theta)$ is from the residue contributions from the half-loops around the poles (clockwise around a pole gives $2\pi i \times$ residue) and a Cauchy principal value integral,

$$\int_{-\infty+i\varepsilon}^{\infty-i\varepsilon} \frac{A}{t-\theta}\,dp = P\int_{C^t_+} \frac{A}{t-\theta}\,dp + \pi i \left.\frac{A}{d\theta/dp}\right|_{p=p_b} - \pi i \left.\frac{A}{d\theta/dp}\right|_{p=p_a}, \tag{15}$$

where P denotes the Cauchy principal value and $p = p_a$ and $p = p_b$ denote the solutions p of $t = \theta$ above and below the real p-axis respectively. The situation for the other integral, resulting from negative frequencies, is shown in Fig. 1b. The contributions from the poles are the same as above but the path of integration in the principal-value integral now runs in the opposite direction. In the total response we see that the principal-value integrals cancel out while the pole contributions add up to give

$$P(t, \mathbf{x}) = \frac{1}{8\pi^2}\left(2\pi i \left.\frac{A}{\mathrm{d}\theta/\mathrm{d}p}\right|_{p=p_4(t)} - 2\pi i \left.\frac{A}{\mathrm{d}\theta/\mathrm{d}p}\right|_{p=p_1(t)}\right) \tag{16}$$

$$= -\frac{1}{2\pi}\,\mathrm{Im}\left(\frac{A}{\mathrm{d}\theta/\mathrm{d}p}\right)_{p=p_4(t)}, \tag{17}$$

where the Cagniard contour is given by $p = p_4(t)$, i.e. the complex p solutions in the lower p-plane. This is the final response.

We have derived the methods used in the subsequent sections in order to show the tunnelling phenomenon.

Tunnelling in a Thin Plane High-velocity Layer

A thin high-velocity layer is a situation which often occurs in practice. We investigate this configuration in detail, showing what effect the thin layer has on the geometrical arrival which occurs when the thin layer is absent. Mellman and Helmberger (1974) also considered this case but their investigation was more of a qualitative than a quantitative nature. The configuration considered is shown in Fig. 2. We assume the media involved to be homogeneous and lossless. The source is above and the receiver below the thin layer. The origin of the coordinate axes is

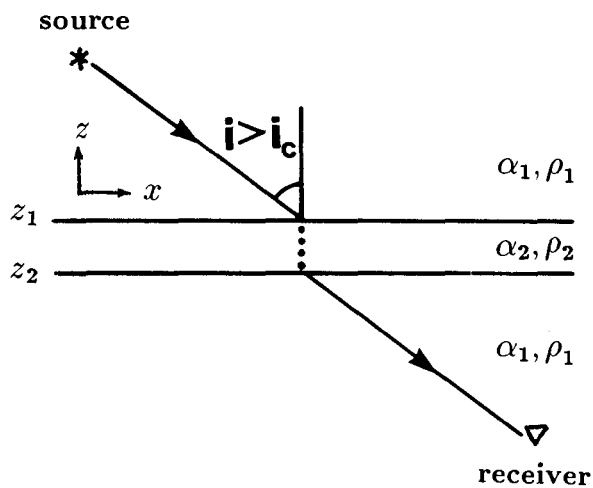

Fig. 2. Thin high-velocity layer embedded in whole space. Geometrical ray impinges at an angle greater than the critical angle on layer. Critical angle i_c.

taken above the upper interface with the z-axis positive upwards. The whole space has a density of ρ_1 and a wave speed of α_1 apart from the thin layer which has a density of ρ_2 and a wave speed of α_2 ($\alpha_2 > \alpha_1$). The subscripts s and r pertain to source and receiver characteristics respectively. The upper interface is at depth z_1, the lower at z_2.

The configuration is plane-layered and thus the ray tracing is unnecessary since the ray parameter remains constant throughout the layers. It is common practice to use propagator matrices to determine the factors A and θ mentioned in the previous section. We did so by making use of the propagator matrices given in Chapman and Orcutt (1985). Let the vertical slowness $q = (1/\alpha^2 - p^2)^{1/2}$.

Then, the thin layer has an overall transmission coefficient T_D given by

$$T_D = \frac{T_{D1} T_{D2} \exp(i\omega q_2(z_1 - z_2))}{1 - R_{U1} R_{D2} \exp(2i\omega q_2(z_1 - z_2))} \tag{18}$$

where T_{D1}, T_{D2}, R_{U1} and R_{D2} are the normalized transmission and reflection coefficients for vertical flux at the single interfaces, i.e.

$$T_{D1} = T_{D2} = \frac{(2\rho_1 q_1)^{1/2}(2\rho_2 q_2)^{1/2}}{\rho_1 q_2 + \rho_2 q_1} \tag{19}$$

$$R_{U1} = R_{D2} = \frac{\rho_1 q_2 - \rho_2 q_1}{\rho_1 q_2 + \rho_2 q_1}. \tag{20}$$

The subscripts U and D pertain to up- and down-going rays respectively. We see that we have still propagation factors exp (...) in the denominator of the transmission coefficient T_D. We can expand the denominator and obtain

$$T_D = T_{D1} T_{D2} \exp(i\omega q_2(z_1 - z_2)) \left\{ \sum_{m=0}^{\infty} (R_{U1} R_{D2})^m \exp(2mi\omega q_2(z_1 - z_2)) \right\}. \tag{21}$$

Each term can be recognized as a multiply-reflected wave. This procedure is a standard one, called the ray expansion. This is an important step since without it we cannot use Cagniard-like methods of inverting to the space–time domain. Each term in this expansion is now in a suitable form for inversion to the time domain using the generalized ray method. And thus, we can use the analytical results of the previous section. For each generalized ray, we have

$$\hat{P}(\omega, p) = \frac{i}{2\omega} A \exp(i\omega\tau), \tag{22}$$

in which

$$A = T_{D1} T_{D2} (R_{U1} R_{D2})^m, \tag{23}$$

$$\tau = q_1 h + (2m + 1) q_2 d, \tag{24}$$

$$h = (z_s - z_r) - (z_1 - z_2), \tag{25}$$

$$d = z_1 - z_2. \tag{26}$$

The Cagniard contour for each of these generalized rays is given by

$$\theta = px + q_1 h + (2m + 1)q_2 d. \tag{27}$$

The result we have obtained here is exact, due to the assumption of plane homogeneous layers. In order to appreciate the tunnelling phenomenon, consider a particular configuration in which the thin layer has a higher wave speed than its surroundings ($\alpha_2 > \alpha_1$). Also assume the layer thickness to be small compared to the source–receiver height ($d \ll h$) and assume the receiver to be at a relatively large distance. A further specification of this latter assumption can be made later on; at the moment we only want to ensure a so-called post-critical (i.e. the incident angle is greater than the critical angle) reflection or transmission.

These specifications will assure that typical Cagniard contours, consisting of the complex solutions $p = p(t)$ which solve $\theta(p) = t$, will be as given in Fig. 3 for different values of m. Only the solutions in the first quadrant are given. They all show the same two features, the first being the part of the curve where it departs from the real p-axis. This corresponds to a combined contribution of a head wave type and a geometrical arrival and has been thoroughly investigated by Drijkoningen and Chapman (1988) and Drijkoningen (1989).

The other feature on the curve is the bend, separated from the point discussed in the previous paragraph, by an inflection point. This is the part in which we are interested since it gives us the tunnelling ray. The number of inflection points give an indication of how many tunnelling rays there will be. For our simple configu-

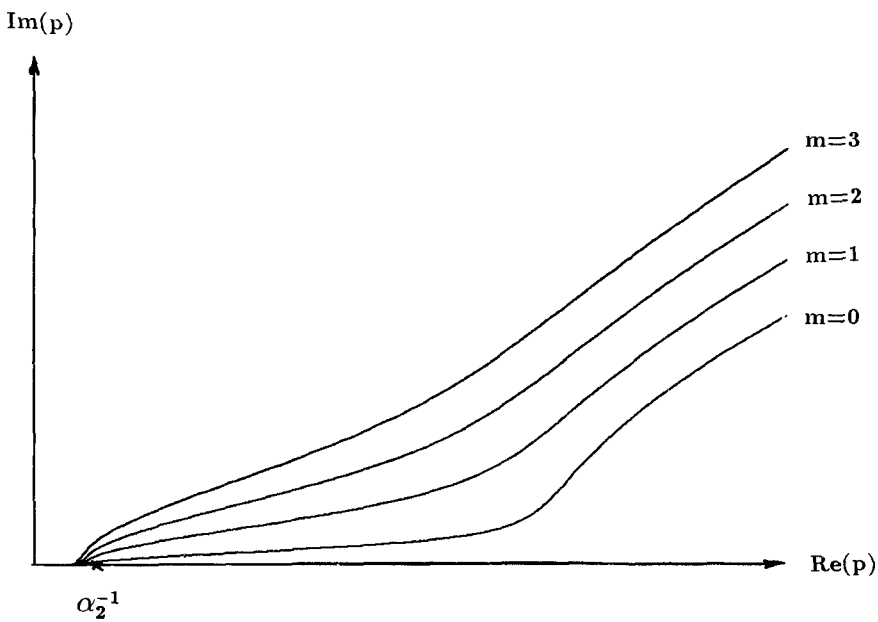

FIG. 3. Cagniard contours $t = px + q_1 h + (2m + 1)q_2 d$ in first quadrant of complex p-plane for different values of m. Note important features: intersection with real p-axis (geometrical arrival) and bend (non-geometrical arrival).

ration of one layer, there are only two inflection points but for more complicated configurations there can be many more.

In Fig. 3, the bend lies near the point on the real p-axis which would be the saddle-point value of the incident field if the thin layer was not there. We expand about this point since the exact analytical expression for the Cagniard contour will be rather complicated. Let this point be p_2 where

$$p_2 = \frac{x}{[x^2 + (h + (2m + 1)d)^2]^{1/2}} \frac{1}{\alpha_1}. \tag{28}$$

In order to expand the vertical slownesses about this value, we set $p = p_2 + \varepsilon$. Then

$$\theta \simeq p_2 x + \bar{q}_1 h + \mathrm{i}(2m + 1)\bar{Q}_2 d + \varepsilon(x - hp_2/\bar{q}_1 - p_2(2m + 1)d/\mathrm{i}\bar{Q}_2) - \varepsilon^2\left(\frac{h}{2\alpha_1^2\bar{q}_1^3} - \frac{(2m + 1)d}{2\alpha_2^2\mathrm{i}\bar{Q}_2^3}\right), \tag{29}$$

in which a bar above a quantity denotes that it is evaluated at p_2 and $\bar{Q}_2 = (p_2^2 - 1/\alpha_2^2)^{1/2}$. Note that q_2 becomes imaginary at p_2, so we have written it as $\mathrm{i}\bar{Q}_2$ where $\bar{Q}_2$ is real. We have

$$p_2 \simeq \frac{x}{R}\frac{1}{\alpha_1}, \qquad R^2 = x^2 + h^2, \tag{30}$$

since $d \ll h$.

Also,

$$\frac{(2m + 1)d}{\bar{Q}_2} \ll \frac{h}{\bar{q}_1}. \tag{31}$$

This implies that we have not included any geometrical spreading effect from the tunnelling path. Hence,

$$\theta \simeq \frac{R}{\alpha_1} + \mathrm{i}(2m + 1)\bar{Q}_2 d - \varepsilon^2 \frac{h}{2\alpha_1^2\bar{q}_1^3}. \tag{32}$$

Notice that to obtain (32) we repeated the expansion, this time not around p_2 but around a nearby point at which the ε term in (29) is zero. It is easy to show that the effect on other terms is negligible due to the assumptions made. The point p_2 around which the expansion in (29) is made, does not lie on the contour. This is obvious since we equate θ to t and, because t is real, we cannot expect to obtain p values on the contour $(R/\alpha_1 + \mathrm{i}(2m + 1)\bar{Q}_2 d$ which give a complex arrival time as obtained above. Solving the contour for the small parameter ε, we obtain

$$\varepsilon = -\mathrm{i}\alpha_1\bar{q}_1\left(\frac{2\bar{q}_1}{h}\right)^{1/2}(t - R/\alpha_1 - \mathrm{i}(2m + 1)\bar{Q}_2 d)^{1/2}. \tag{33}$$

We then expand $\mathrm{d}\theta/\mathrm{d}p$ about p_2, giving

$$\mathrm{d}\theta/\mathrm{d}p \simeq -\varepsilon \frac{h}{\alpha_1^2\bar{q}_1^3}. \tag{34}$$

We substitute ε from (33) into $d\theta/dp$, and then separate the root of the complex quantity in ε into a real and imaginary part which is easily done (Drijkoningen and Chapman 1988).

The amplitude term behaves smoothly near p_2 so it can be evaluated at p_2 and treated as a constant. It is convenient to write

$$\rho_2 \bar{q}_1 + i\rho_1 \bar{Q}_2 = |s| e^{i\phi}. \tag{35}$$

Then each amplitude term in (21) can be written as

$$T_{D1} T_{D2} (R_{U1} R_{D2})^m = i \frac{4\rho_1 \rho_2 \bar{q}_1 \bar{Q}_2}{|s|^2} \exp\{-2i\phi(2m+1)\}. \tag{36}$$

Using this expression for each m and adding all the contributions gives the approximate response for the line-source problem

$$\begin{aligned} P^{\text{trans}}(t, \mathbf{x}) \simeq \frac{1}{2\pi^2} \frac{4\rho_1 \rho_2 \bar{q}_1 \bar{Q}_2}{|s|^2} \bar{q}_1 \left(\frac{\alpha_1}{2R}\right)^{1/2} \\ \times \left\{ \frac{H(t - R/\alpha_1)}{(t - R/\alpha_1)^{1/2}} * \sum_{m=0}^{\infty} \frac{(2m+1)\bar{Q}_2 d}{t^2 + (2m+1)^2 \bar{Q}_2^2 d^2} \sin 2\phi(2m+1) \right. \\ \left. + \frac{H(R/\alpha_1 - t)}{(R/\alpha_1 - t)^{1/2}} * \sum_{m=0}^{\infty} \frac{-(2m+1)\bar{Q}_2 d}{t^2 + (2m+1)^2 \bar{Q}_2^2 d^2} \cos 2\phi(2m+1) \right\}, \end{aligned} \tag{37}$$

where the asterisk $*$ denotes convolution. For a full derivation, see Drijkoningen and Chapman (1988). This is the expression we wished to obtain.

The most important feature in (37) is revealed when we transform the time-dependent part in the sums to the frequency domain, namely

$$\mathscr{F}_t \left\{ \frac{(2m+1)\bar{Q}_2 d}{[t^2 + (2m+1)^2 \bar{Q}_2^2 d^2]^{1/2}} \right\} = \pi \exp(-\omega(2m+1)\bar{Q}_2 d), \tag{38}$$

for $\omega > 0$. The tunnelling part is represented by an exponentially decaying part in the frequency domain.

The other characteristics can also be easily derived from the above expressions. Firstly these are two terms due to the transmission factor having a real and an imaginary part at p_2, one giving rise to a smoothed incident-field term, the other giving a smoothed Hilbert-transformed incident field (i.e. reversed in time). Secondly the approximate signal is acausal, although, the exact response of the generalized ray method before expansion about p_2 is not. Finally, the tunnelling ray only exists in a certain limited region in space. This is contained in the assumption that $q_2(p_2)$ becomes imaginary when the receiver is at a distance large compared to the source and receiver heights.

We now assess the approximation we have taken by comparing the exact and approximate results numerically. In the following figures we have taken a finite sampling width to smooth the results. The result of the generalized ray method contains an inverse square root singularity at the arrival time of the geometrical arrival time but due to the numerical smoothing the singularity may not show. Also,

due to this numerical smoothing the tangent at the point of intersection of the contour with the real p-axis is not completely parallel to the imaginary axis.

First consider the first term of the expansion above ($m = 0$). Both the contour and the time response show the same behaviour as for the tunnelled ray as discussed in Drijkoningen and Chapman (1988). In Fig. 4 we show the exact response for a

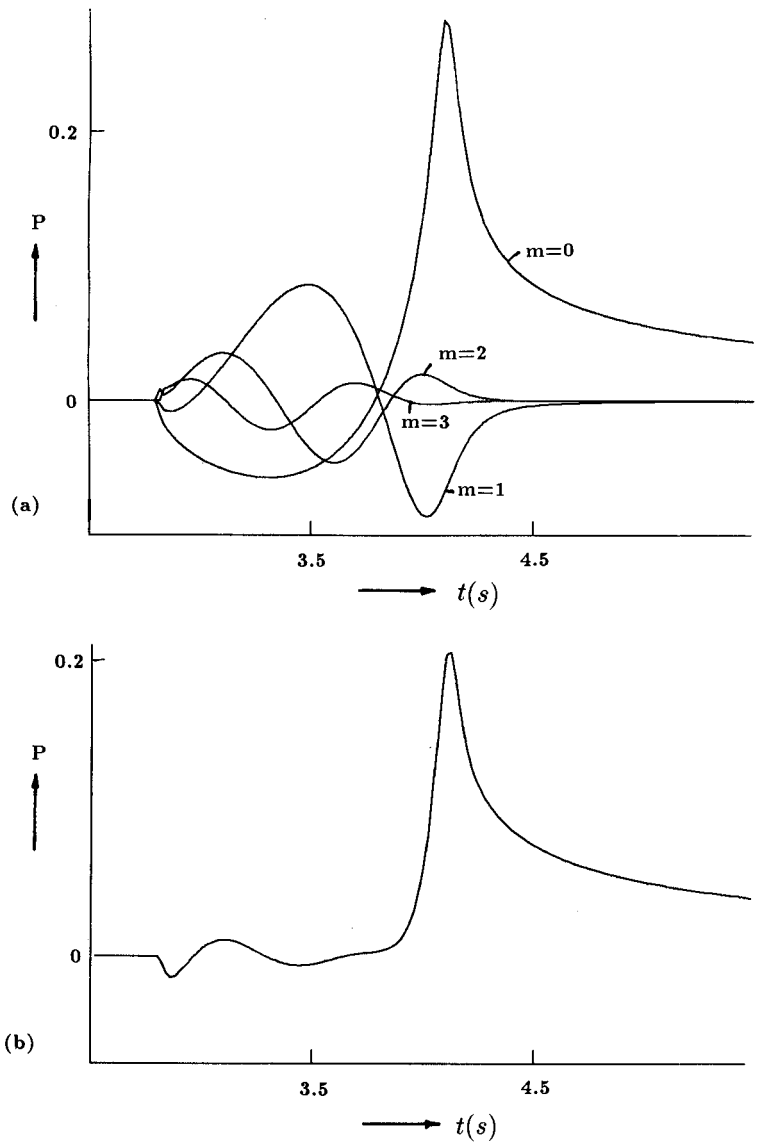

FIG. 4. Signal for line-source excitation for thin layer in homogeneous region. $x = 6$ km, $z_1 = -1$ km, $z_2 = -1.1$ km, $z_3 = -1.5$ km, $\alpha_2/\alpha_1 = 2$, $\rho_2/\rho_1 = 1.2$. (a) Separate rays for various numbers m; (b) stacked response up to $m = 3$; (c) *idem* up to $m = 10$.

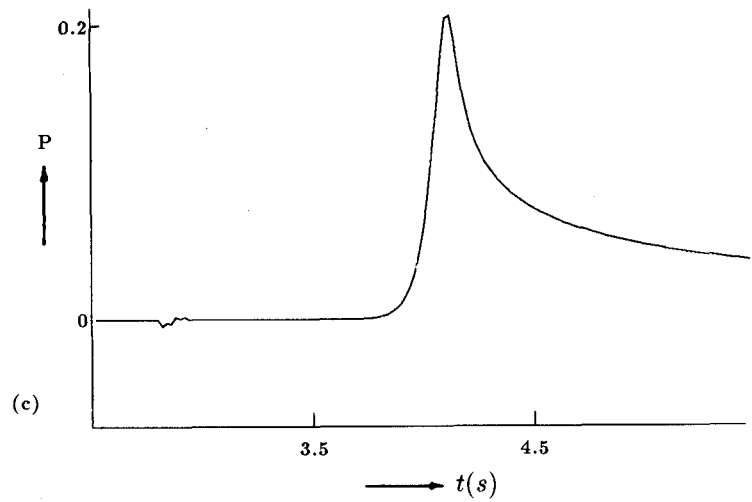

FIG. 4 (*continued*).

high-impedance contrast ($\rho_2\alpha_2/\rho_1\alpha_1 = 2.4$). Note the two contributions before and after the geometrical-arrival time. They are due to the fact that the arrival for each m consists of two contributions. It is now interesting to see what happens when we increase the number m. In Fig. 4a we can see that increasing m gives a more rapidly varying response in the time domain. This behaviour occurs due to the factor $(R_{U1}R_{D2})^m$ which, for complex values, we have written as in (36). It includes the factor $\exp(-2i\phi(2m+1))$. The rapidly varying behaviour is now obvious when m becomes large.

In the added (total) response we can see that the different rays interfere with each other in a specific way. Real rays will arrive at different times at the receiver and the total response will be a succession of arrivals, but for tunnelling ray the arrivals are hardly separated in time and will interfere with each other. Thus the summed total response can be interpreted as a beam: an infinite sum of separate rays. The total response will be one arrival which contains the contribution from all the tunnelling rays. From Fig. 4 it can be seen that the non-geometrical arrival is not very different from the response due to tunnelling only once ($m = 0$). The inclusion of all the multiples will make the waveform of the evanescent waves approach the function $H(t)t^{-1/2}$, which we would expect on physical grounds.

The head-wave-type arrival, however, changes drastically when we add many multiples. The original head-wave-type behaviour from $m = 0$ almost completely disappears. This behaviour has been mentioned by Mellman and Helmberger (1974), who called it precursory noise to the seismogram. In Fig. 5 we have increased the thickness of the layer and have included more multiples in Fig. 5b. In Fig. 6 we compare the exact response from Fig. 4c with the approximate response. We can see that it models the exponential decay in the frequency domain (which determines the

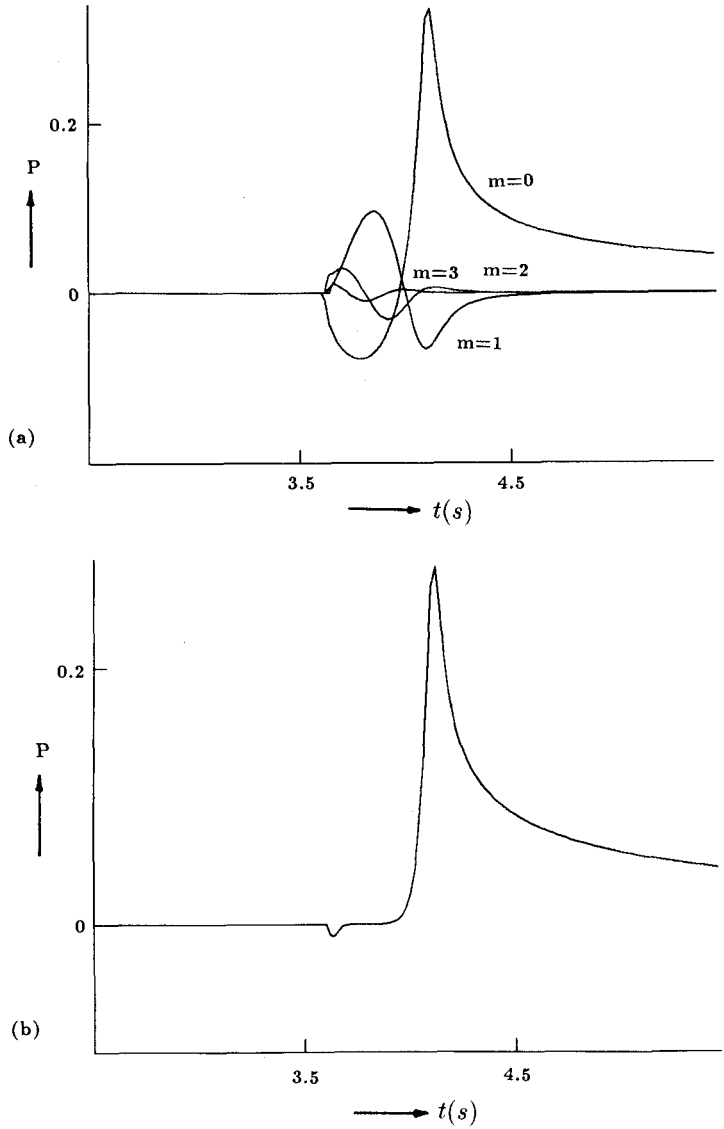

FIG. 5. Signal for line-source excitation for thin layer in homogeneous layer. $z_2 = 1.3$ km, other parameters same as in Fig. 4. (a) Separate rays; (b) up to $m = 10$ stacked.

wave shape) fairly well, apart from a d.c. value difference between the two. However, such a d.c. value does not influence the shape of the signal.

In Fig. 7 we show a number of traces in order to see how these features will behave at different ranges. Before the critical range the time differences between different arrivals are so small that the sum of arrivals is almost equal to a large-

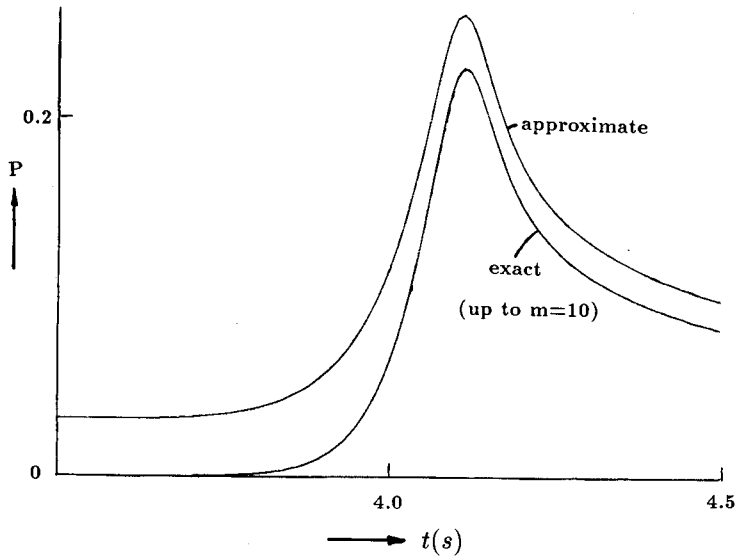

FIG. 6. Comparison of Fig. 4c with the approximate response as derived in text.

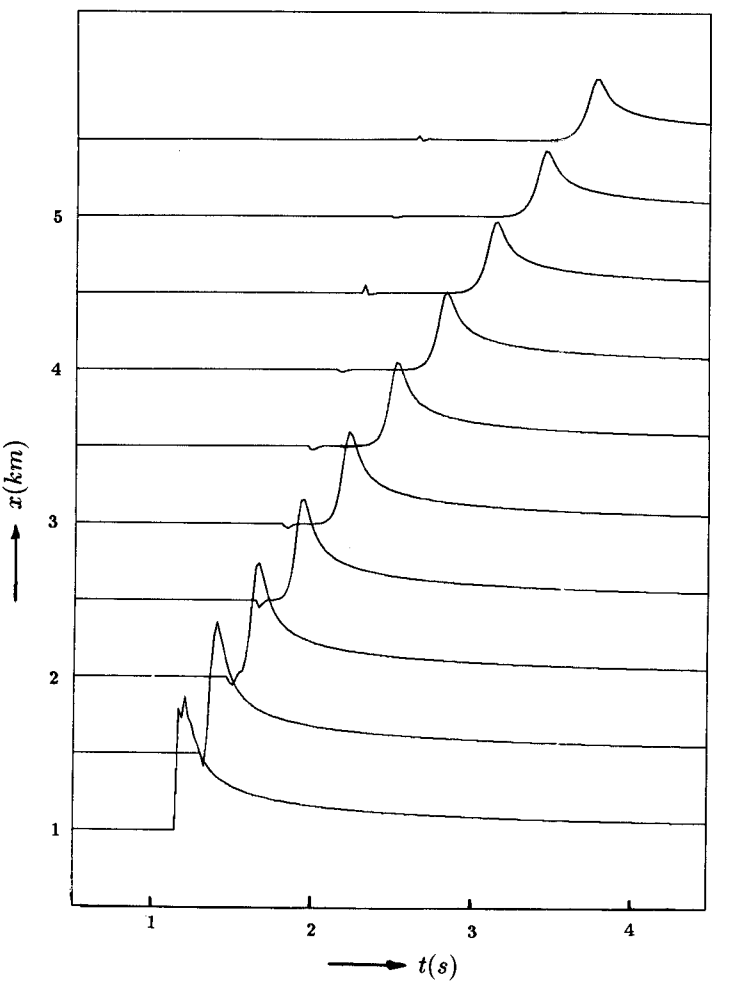

FIG. 7. Ten traces to show all features discussed in section on tunnelling in thin high-velocity layer. Parameters as in Fig. 4. 10 multiples within layer included.

amplitude arrival. Beyond the critical range the tunnelling rays add up to give a smooth arrival while the head-wave-type arrivals remain of a small amplitude due to the cancelling as discussed above. The change in the head-wave-type arrival across the ranges is due to the finite sampling width applied in the examples.

Tunnelling in Regions Separated by Dipping Interfaces

We now derive the formula for the case of layers with dipping interfaces. We follow Diebold (1987) in deriving the formula for the simple configuration as shown in Fig. 8. We choose the origin of the coordinate axes at the source in order to reduce the algebra. The receiver is, for convenience, taken at the same level as the source. We designate the source–receiver range as x and the depths at which the interfaces cross the vertical reference line, say $x = 0$, as z_i. These coordinates depend only on the configuration. We then introduce the coordinates X_i and Z_i in order to denote the depths and ranges at which the ray crosses the consecutive interfaces. There is no need to determine these explicitly since they will cancel out in the final result. In each homogeneous 'layer' we define horizontal and vertical slownesses, i.e. the ray vector, with reference to the global coordinate axes. A subscript to a component of the slowness will designate the number of the layer according to Fig. 8 and a superscript U or D denotes whether the horizontal or vertical slowness corresponds to an up- or down-going ray, respectively. The first step in the derivation of the space-time formula is forming the traveltime function as

$$\theta(p_1^{\mathrm{D}}, p_2^{\mathrm{D}}, p_2^{\mathrm{U}}, p_1^{\mathrm{U}}) = p_1^{\mathrm{D}}X_1 + p_2^{\mathrm{D}}(X_2 - X_1) + p_2^{\mathrm{U}}(X_3 - X_2) + p_1^{\mathrm{U}}(x - X_3) + q_1^{\mathrm{D}}Z_1 + q_2^{\mathrm{D}}(Z_2 - Z_1) - q_2^{\mathrm{U}}(Z_3 - Z_2) - q_1^{\mathrm{U}}(0 - Z_3) \tag{39}$$

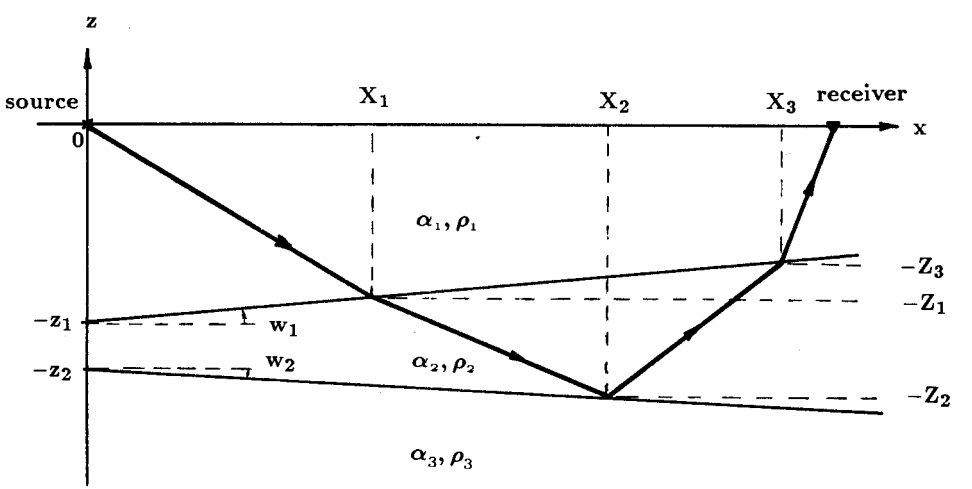

FIG. 8. Configuration with two dipping interfaces. Range denoted by x and depths at which interfaces cross line $x = 0$ denoted by z_i. Coordinates X_i and Z_i are (artificial) coordinates at which ray crosses interfaces.

(compare with (27)). Since we are dealing with dipping layers, the horizontal slownesses are not the same on every section of the raypath. We notice that the depths of the interfaces change with offset, i.e.

$$-Z_1 = -z_1 + X_1 \tan w_1, \tag{40}$$

$$-Z_2 = -z_2 + X_2 \tan w_2, \tag{41}$$

$$-Z_3 = -z_1 + X_3 \tan w_1. \tag{42}$$

Substituting these values in (39) and grouping terms with X_i, $X_i \tan w_j$ and z_i gives

$$\begin{aligned}\theta(p_1^{\mathrm{D}}, p_2^{\mathrm{D}}, p_2^{\mathrm{U}}, p_1^{\mathrm{U}}) = {} & X_1(p_1^{\mathrm{D}} - p_2^{\mathrm{D}}) + X_2(p_2^{\mathrm{D}} - p_2^{\mathrm{U}}) + X_3(p_2^{\mathrm{U}} - p_1^{\mathrm{U}}) \\ & - X_1 \tan w_1(q_1^{\mathrm{D}} - q_2^{\mathrm{D}}) - X_2 \tan w_2(q_2^{\mathrm{D}} + q_2^{\mathrm{U}}) \\ & - X_3 \tan w_1(q_1^{\mathrm{U}} - q_2^{\mathrm{U}}) + p_1^{\mathrm{U}} x + z_1(q_1^{\mathrm{D}} - q_2^{\mathrm{D}}) \\ & + z_2(q_2^{\mathrm{D}} + q_2^{\mathrm{U}}) + z_1(q_1^{\mathrm{U}} - q_2^{\mathrm{U}}).\end{aligned} \tag{43}$$

Applying Snell's law at the interfaces will cancel out the first six terms. Snell's law and some associated expressions needed for the final response are given in the Appendix. Let us consider the case of a transmission across an interface (case (a) in the Appendix). Snell's law requires that across the interface

$$\alpha_1^{-1} \sin(a_1 - w_1) = \alpha_2^{-1} \sin(a_2 - w_1), \tag{44}$$

where a_1 and a_2 are the angles of the rays with the global z-axis. Writing out the sines and recognizing $\alpha_1^{-1} \sin a_1$ as p_1^{D}, $\alpha_1^{-1} \cos a_1$ as q_1^{D}, $\alpha_2^{-1} \sin a_2$ as p_2^{D} and $\alpha_2^{-1} \cos a_2$ as q_2^{D}, we get

$$p_1^{\mathrm{D}} - q_1^{\mathrm{D}} \tan w_1 = p_2^{\mathrm{D}} - q_2^{\mathrm{D}} \tan w_1. \tag{45}$$

This relation causes the first and fourth terms to cancel out in the above function of θ. The same can be done for the other cases, see Appendix. These relations then give the expression for θ

$$\theta(p_1^{\mathrm{D}}) = p_1^{\mathrm{U}} x + q_1^{\mathrm{D}} z_1 + q_2^{\mathrm{D}}(z_2 - z_1) + q_2^{\mathrm{U}}(z_2 - z_1) + q_1^{\mathrm{U}} z_1. \tag{46}$$

Thus we only have to specify the coordinates of the configuration at a fixed reference line. It should be noted that θ is a function of p_1^{D} only, since all the other terms are dependent on p_1^{D} via Snell's law at the interfaces.

We have illustrated the configuration with two dipping interfaces, but it is easy to see that the derivation can be performed for any number of interfaces. The θ function then becomes

$$\theta(p_1^{\mathrm{D}}) = p_1^{\mathrm{U}} x + \sum_i \{q_i^{\mathrm{D}}(z_i - z_{i-1}) + q_i^{\mathrm{U}}(z_i - z_{i-1})\}, \tag{47}$$

where, again, we have assumed that the reference line is at the source, i.e. $x = 0$.

We must now determine the geometric spreading effect by including information from neighbouring rays, since we have an explicit expression for the θ function which includes all the information from the ray equations, namely, that for homogeneous regions rays are straight lines in space and satisfy Snell's law at interfaces, we

do not need to determine the geometric spreading effect explicitly. In ART, geometric spreading is usually obtained by perturbing the ray equations and solving the resulting system. In the formulation followed here, perturbing the θ function is equivalent to perturbing the ray equations since θ includes all the information from the ray equations.

In the determination of the response, we must also consider the amplitude coefficients due to transmission or reflection at an interface. This procedure is standard in ART (see e.g. Červený and Ravindra 1971). At an interface we set up a local normal and determine the reflection or transmission coefficient with the *local* coordinate system. For instance, for the transmission of a downgoing ray we get

$$T_{\mathrm{D}} = \frac{(2\rho_1 q_{n1}^{\mathrm{D}})^{1/2}(2\rho_2 q_{n2}^{\mathrm{D}})^{1/2}}{\rho_1 q_{n2}^{\mathrm{D}} + \rho_2 q_{n1}^{\mathrm{D}}}, \tag{48}$$

where

$$q_{ni}^{\mathrm{D}} = q_i^{\mathrm{D}} \cos w - p_i^{\mathrm{D}} \sin w. \tag{49}$$

The other possibilities can be obtained similarly.

We have now established the relevant formulae for the case of homogeneous layers with dipping interfaces and we have determined the θ function and the amplitude A which includes all reflection and transmission coefficients as well as matching of the wavefield at the source and receiver. Inverting to the space–time domain following the same procedure as in the previous sections, we get, for the line-source problem,

$$P(t, \mathbf{x}) \simeq \frac{1}{4\pi^2} \int_{-\infty}^{\infty}\int_{-\infty}^{\infty} \frac{\mathrm{i}A}{2\omega} \exp\{-\mathrm{i}\omega(t - \theta(p_1^{\mathrm{D}}))\} |\omega| \, \mathrm{d}p_1^{\mathrm{D}} \, \mathrm{d}\omega \tag{50}$$

$$= -\frac{1}{2\pi} \operatorname{Im}\left(\frac{A}{\mathrm{d}\theta/\mathrm{d}p_1^{\mathrm{D}}}\right)_{p=p_4(t)}, \tag{51}$$

where, for the case of two dipping interfaces, A takes the form,

$$A = \left(\frac{\rho_{\mathrm{r}}}{\rho_{\mathrm{s}}}\right)^{1/2} \frac{1}{q_{\mathrm{r}}^{1/2} q_{\mathrm{s}}^{1/2}} T_{\mathrm{D1}} R_{\mathrm{D2}} T_{\mathrm{U1}}. \tag{52}$$

This is the required result.

Before proceeding we must show that this expression includes the geometric spreading effect. Thus we expand the contour about the value of the geometrical arrival, i.e. that value which makes $\mathrm{d}\theta/\mathrm{d}p_1^{\mathrm{D}}$ zero, say p_{s}. Taking $p_1^{\mathrm{D}} = p = p_{\mathrm{s}} + \varepsilon$ where ε is a small quantity, we get

$$\theta \simeq T_{\mathrm{s}} + \frac{1}{2}\varepsilon^2 \left.\frac{\mathrm{d}^2\theta}{\mathrm{d}p^2}\right|_{p=p_{\mathrm{s}}}, \tag{53}$$

where T_{s} is the arrival time of the geometrical arrival. Solving for ε gives

$$\varepsilon = \frac{(\theta - T_{\mathrm{s}})^{1/2} 2^{1/2}}{(\mathrm{d}^2\theta/\mathrm{d}p^2 \,|_{p=p_{\mathrm{s}}})^{1/2}}. \tag{54}$$

Expanding $\mathrm{d}\theta/\mathrm{d}p$ about p_s and substituting ε from (54) gives

$$\frac{\mathrm{d}\theta}{\mathrm{d}p} \simeq \varepsilon \left.\frac{\mathrm{d}^2\theta}{\mathrm{d}p^2}\right|_{p=p_s}$$

$$= (\theta - T_s)^{1/2} 2^{1/2} \left(\frac{\mathrm{d}^2\theta}{\mathrm{d}p^2}\right)^{1/2}_{p=p_s}. \tag{55}$$

It is now possible to show that $(\mathrm{d}^2\theta/\mathrm{d}p^2)^{1/2}$ at the saddle point is associated with the geometrical spreading effect, but since the algebra is tedious and awkward we refer to Hong and Helmberger (1978) who showed this equivalence. Here, it is enough to say that the above expression does include geometric spreading.

For the numerical implementation we need some extra expressions which follow from the results of the last section and can be used as final expressions in a numerical scheme. We start off with rays from the source, i.e. with p_1^{D} in the example of two dipping interfaces. We need to know the horizontal or vertical slowness in the next layer in terms of the present values since we need to know the vertical slowness in the expression for $\theta(p_1^{\mathrm{D}})$ in (47). It is a matter of choice whether we first determine the vertical or horizontal slowness in terms of the present values. We have chosen the horizontal slowness since for plane layering, the expression should give a horizontal slowness which is constant across an interface. The rays in the next layer must be expressed in terms of this source ray, connecting the rays at the interface using Snell's law. The transmission of a downgoing ray is given by (45). This can be solved for p_2^{D}, i.e.

$$p_2^{\mathrm{D}} = \frac{p_1^{\mathrm{D}} - q_1^{\mathrm{D}} \tan w}{1 + \tan^2 w} + \frac{\tan w}{1 + \tan^2 w} \{\alpha_2^{-2}(1 + \tan^2 w) - (p_1^{\mathrm{D}} - q_1^{\mathrm{D}} \tan w)^2\}^{1/2}. \tag{56}$$

We have chosen the root which satisfies Snell's law. This expression is included in the Appendix. The expressions for the other possibilities of reflections and transmissions are also given in the Appendix, as is the differentiation of the transmitted or reflected ray with respect to the incident ray. In the final expression of the generalized ray method, the term $\mathrm{d}\theta/\mathrm{d}p_1^{\mathrm{D}}$ is present. Performing this differentiation gives us terms such as $\mathrm{d}p_2^{\mathrm{D}}/\mathrm{d}p_1^{\mathrm{D}}$, $\mathrm{d}p_1^{\mathrm{U}}/\mathrm{d}p_1^{\mathrm{D}}$, etc. These expressions for the various possibilities of reflections and transmissions are included in the Appendix.

We shall now give some numerical examples, illustrating the previous results. Examples of this kind have been computed before, e.g. by Hong and Helmberger (1977, 1978), although their theory lacked rigour and generality and their formula for the θ function was not as simple as the one we have used, namely following Diebold (1987).

The first example is straightforward and consists of two dipping interfaces as discussed above. At the base of the model we have a medium with a relatively high velocity. The synthetic seismograms are given in Fig. 9. At a certain range this will give rise to head waves. The traveltimes for head waves and geometrical rays in dipping layers are well known (see e.g. Dobrin 1976; Kearey and Brooks 1984) and can of course be deduced from the formulae above. The classical results only give traveltimes but with a method like the generalized ray method, we are able to

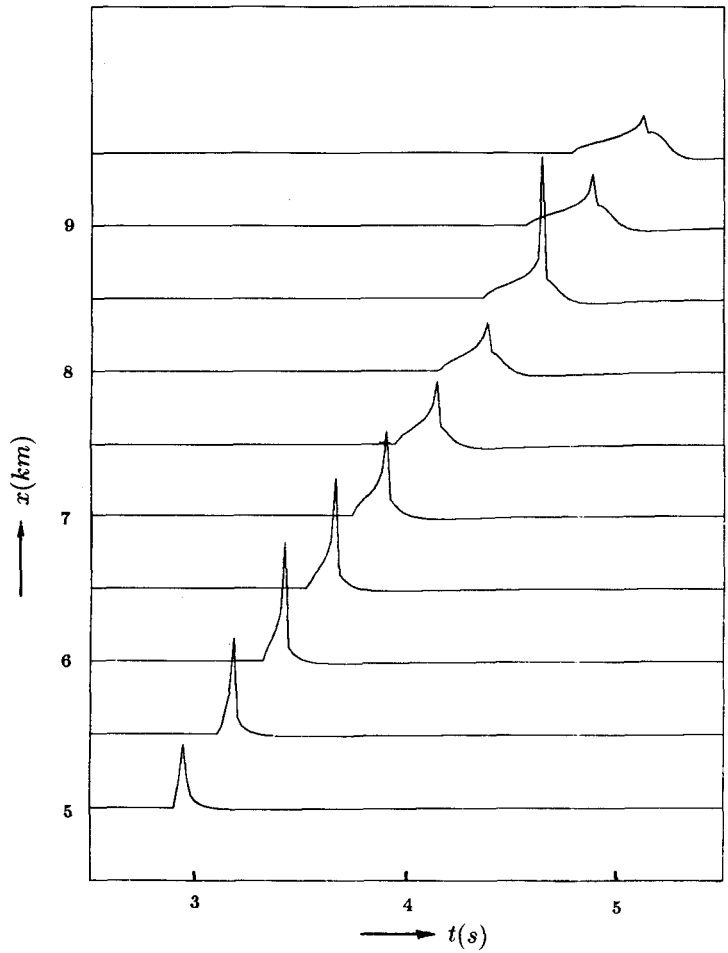

FIG. 9. Synthetic seismograms for configuration in Fig. 8. $z_1 = 1$ km, $z_2 = 1.3$ km, $\tan w_1 = 0.05$, $\tan w_2 = -0.03$, $\alpha_2/\alpha_1 = 0.9$, $\alpha_3/\alpha_1 = 1.25$, $\rho_2/\rho_1 = 1.2$, $\rho_3/\rho_1 = 1$.

obtain more information from the structure below, such as geometrical spreading and waveform.

The next example is a dipping high-velocity layer embedded in a homogeneous layer (Fig. 10). In the light of the previous section of tunnelling with non-dipping interfaces, the results are easy to interpret. The layer being thin, the tunnelling can be very significant as shown in Fig. 11. As the layer becomes thicker, the evanescent wave becomes less significant until it eventually disappears. In the final figures we did not include any multiple reflections and thus the head-wave-type arrival has a rather large amplitude. As shown in the previous section, the inclusion of multiple

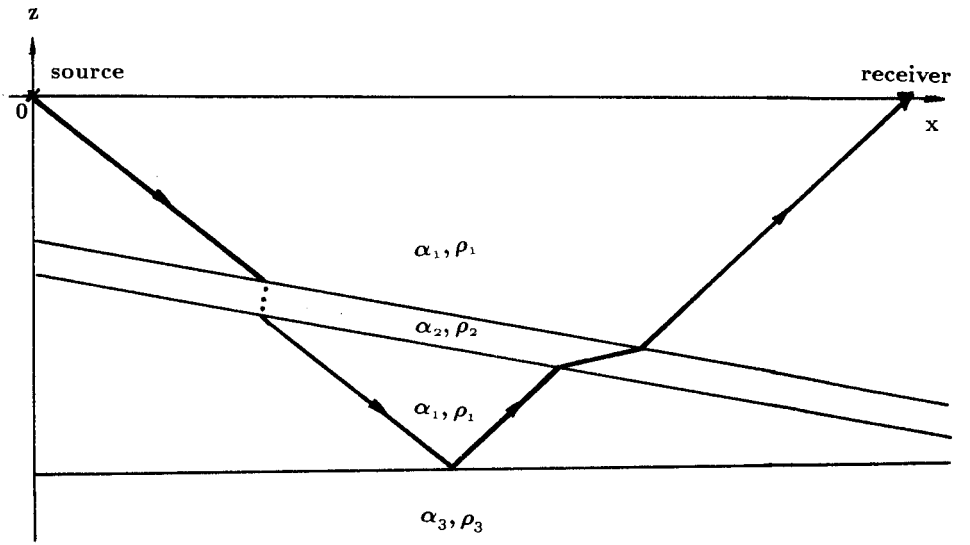

FIG. 10. Thin dipping layer embedded in homogeneous layer.

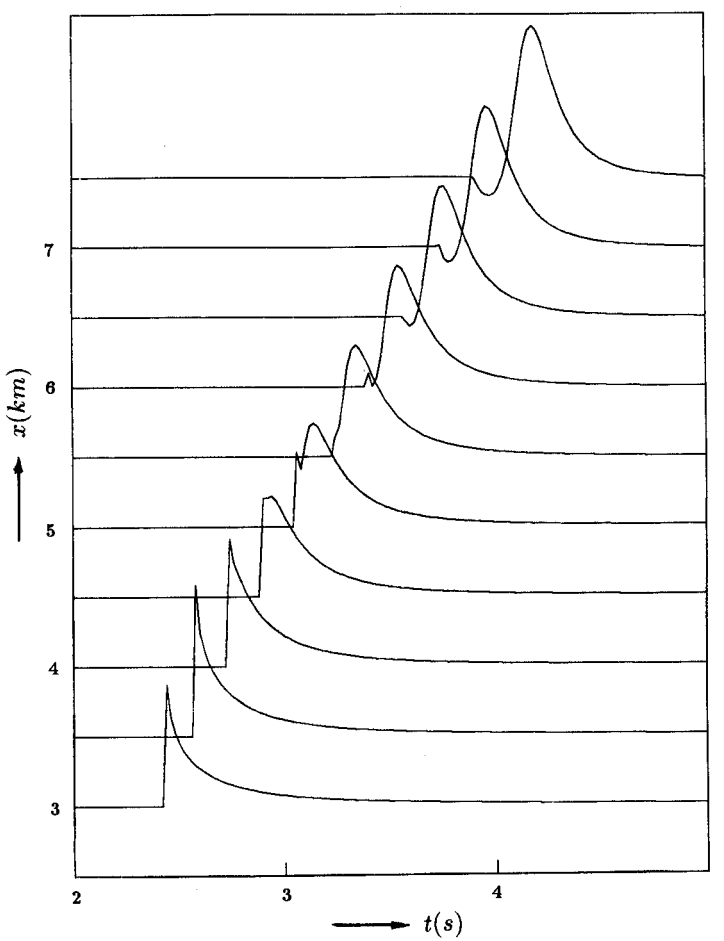

FIG. 11. Synthetic seismograms for thin dipping layer. $z_1 = 1$ km, $z_2 = 1.1$ km, $z_3 = 2$ km, $\tan w_1 = \tan w_2 = -0.1$, $\tan w_3 = 0.02$, $\alpha_2/\alpha_1 = 1.33$, $\alpha_3/\alpha_1 = 1.2$, $\rho_2/\rho_1 = 1.2$, $\rho_3/\rho_1 = 1$.

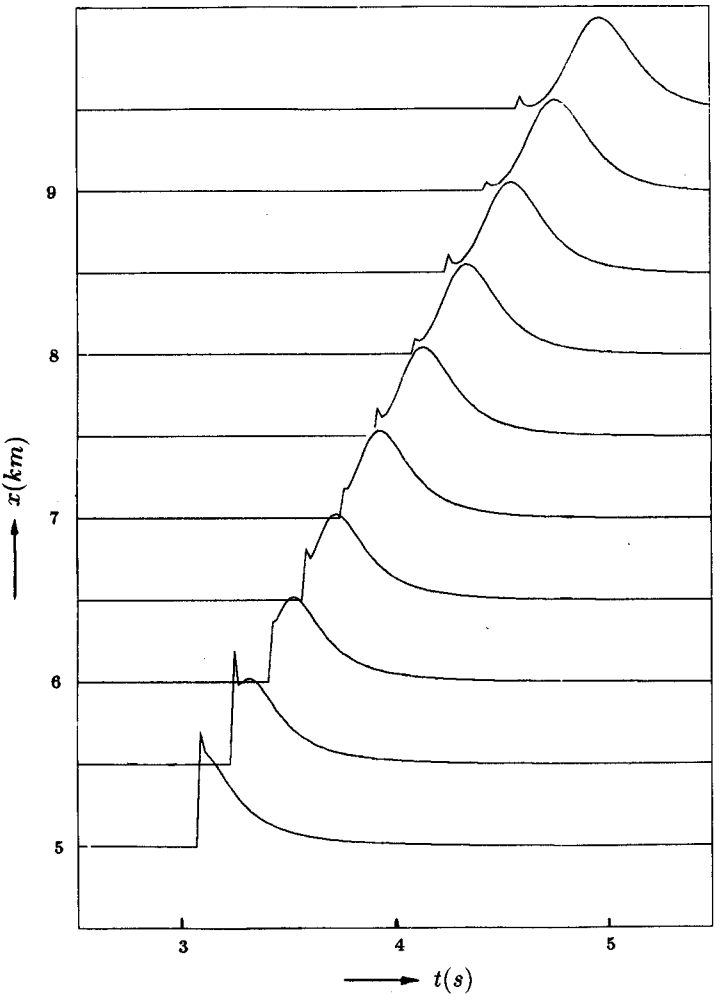

FIG. 12. Synthetic seismograms for thin layer wedging out. $z_1 = 1.3$ km, $z_2 = 1.4$ km, $z_3 = 2$ km, $\alpha_2/\alpha_1 = 1.33$, $\alpha_3/\alpha_1 = 1.2$, $\tan w_1 = 0.1$, $\tan w_2 = 0.02$, $\tan w_3 = -0.02$, $\rho_2/\rho_1 = 1.2$, $\rho_3/\rho_1 = 1$.

reflections within the thin layer will cause this arrival to disappear almost completely. The evanescent wave shows the same behaviour as in the plane-layer case. Although we did not include any multiple reflections, which will modify the amplitude slightly, we have illustrated our point that tunnelling is indeed modelled by our approach.

Figure 12 shows the seismograms for a model consisting of a thin layer wedging out in the positive x direction. Again, all the features which were mentioned before can be discerned in the figure.

Discussion

In the previous sections we have seen how to obtain the tunnelling ray using the generalized ray method. At the start of the discussion we extended the generalized ray method to include the possibility of laterally inhomogeneous media. Although we only used it for media which were homogeneous, it is also possible to include velocity gradients in the models, but we must be careful to include the possibility of turning rays. However, a disadvantage of the method remains in that we must have an explicit expression for the contour $t = \theta$. For geometrical arrivals it is preferable to use Champan's (WKBJ seismogram) method in which we construct the θ curve by 'shooting' rays. This is particularly useful for complicated structures. The method of obtaining the p value in the generalized ray method has some similarity to the method known as 'bending'. It should however be remembered that we cannot model the tunnelling as discussed here using Chapman's method (Drijkoningen 1989).

As we have seen, the most important feature of the tunnelling is the complex phase. We can use this characteristic to determine the position of these arrivals in the same way as with real rays. Such an approach is taken in the ART approximation where we begin with a complex phase, i.e. we allow $T(\mathbf{x})$ to be complex in the expansion (4). This gives us the problem known as complex ray tracing. Many problems still exist in dealing with it and it is not clear how to solve even the starting equations (e.g. Keller 1958; Choudhary and Felsen 1973; Felsen 1976; Einziger and Felsen 1982).

Conclusions

We have discussed tunnelling rays in two different configurations. If we use the result of the generalized ray method to produce a synthetic seismogram, the tunnelling ray is automatically included and only needs an interpreter to recognize the arrival as such. The characteristics can be revealed by expanding the response about the ray parameters of interest. The most important feature of the ray is the exponentially decaying part in the frequency domain, or in terms of asymptotic theory, a complex phase. The other characteristics are that the approximate signal is always acausal (while the full generalized ray response is not) and the arrival exists only in a certain limited region in space.

In the first configuration of a thin high-velocity layer we were able to show the arrival clearly. When using an expansion around the ray parameter of interest, the wave shape was modelled very well, but the multiply-tunnelled arrivals within the thin layer caused a considerable d.c. value to exist between the exact and approximate response. In the case of dipping layers we were able to show this tunnelling in some configurations and that it has a considerable amplitude.

Acknowledgements

The author thanks Chris Chapman for many useful comments on the subject and John Hudson who improved the mathematical formulation of the problem. Most of this work was done while the author was supported by a Shell Scholarship (U.K.).

Computations were performed at the Vax computer centre at the Bullard Laboratories, Department of Earth Sciences, Cambridge (U.K.). Department of Earth Sciences No. 1822.

APPENDIX

The expressions used in the generalized ray response in the case of homogeneous media separated by dipping interfaces are given. These expressions follow from Snell's law at a dipping interface. Figure 13 depicts the four possible cases.

(a) Transmission for downgoing ray:

$$\alpha_1^{-1} \sin(a_1 - w) = \alpha_2^{-1} \sin(a_2 - w); \tag{A1}$$

$$\frac{dp_2^D}{dp_1^D} = \frac{1 + \tan w\, p_1^D/q_1^D}{1 + \tan w\, p_2^D/q_2^D}; \tag{A2}$$

$$p_2^D = \frac{p_1^D - q_1^D \tan w}{1 + \tan^2 w} + \frac{\tan w}{1 + \tan^2 w} \times \{\alpha_2^{-2}(1 + \tan^2 w) - (p_1^D - q_1^D \tan w)^2\}^{1/2}. \tag{A3}$$

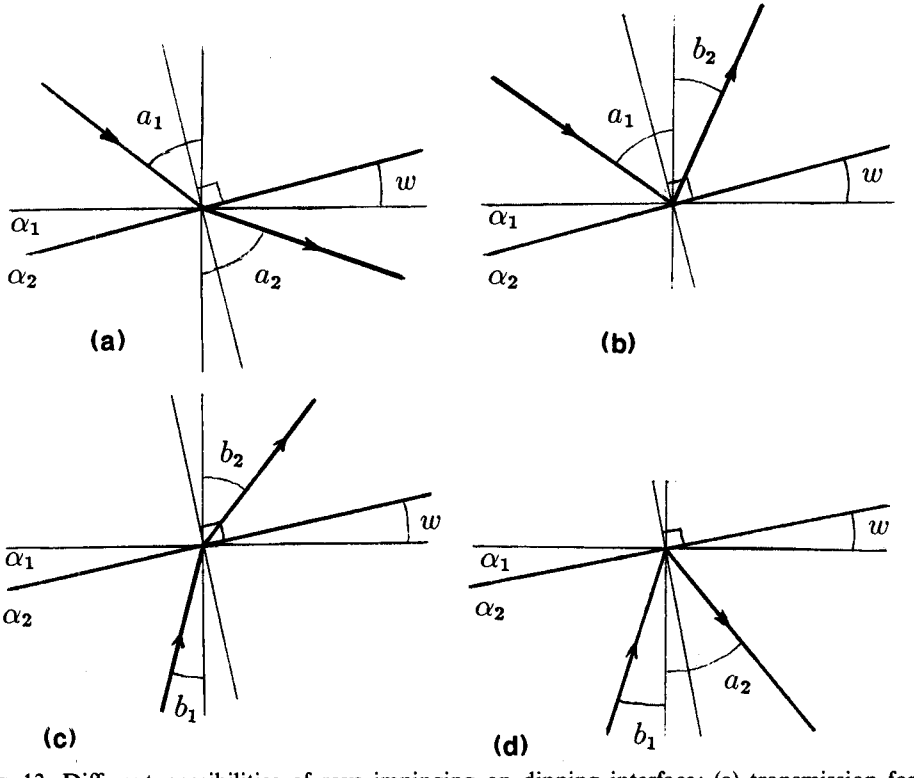

FIG. 13. Different possibilities of rays impinging on dipping interface: (a) transmission for downgoing ray; (b) reflection for downgoing ray; (c) transmission for upgoing ray; (d) reflection for upgoing ray.

(b) Reflection for downgoing ray:

$$\alpha_1^{-1} \sin (a_1 - w) = \alpha_1^{-1} \sin (b_1 + w); \tag{A4}$$

$$\frac{dp_1^U}{dp_1^D} = \frac{1 + \tan w \, p_1^D/q_1^D}{1 - \tan w \, p_1^U/q_1^U}; \tag{A5}$$

$$p_1^U = p_1^D \frac{1 - \tan^2 w}{1 + \tan^2 w} - q_1^D \frac{2 \tan w}{1 + \tan^2 w}. \tag{A6}$$

(c) Transmission for upgoing ray:

$$\alpha_2^{-1} \sin (b_1 + w) = \alpha_1^{-1} \sin (b_2 + w); \tag{A7}$$

$$\frac{dp_1^U}{dp_2^U} = \frac{1 - \tan w \, p_2^U/q_2^U}{1 - \tan w \, p_1^U/q_1^U}; \tag{A8}$$

$$p_1^U = \frac{p_2^U + q_2^U \tan w}{1 + \tan^2 w} - \frac{\tan w}{1 + \tan^2 w} \times \{\alpha_1^{-2}(1 + \tan^2 w) - (p_2^U + q_2^U \tan w)^2\}^{1/2}. \tag{A9}$$

(d) Reflection for upgoing ray:

$$\alpha_2^{-1} \sin (b_1 + w) = \alpha_2^{-1} \sin (a_2 - w); \tag{A10}$$

$$\frac{dp_2^D}{dp_2^U} = \frac{1 - \tan w \, p_2^U/q_2^U}{1 + \tan w \, p_2^D/q_2^D}; \tag{A11}$$

$$p_2^D = p_2^U \frac{1 - \tan^2 w}{1 + \tan^2 w} - q_2^U \frac{2 \tan w}{1 + \tan^2 w}. \tag{A12}$$

REFERENCES

ABRAMOVICI, F., LE, L.H.T. and KANASEWICH, E.R. 1989. The evanescent wave in Cagniard's problem for a line source generating SH waves. *Bulletin of the Seismological Society of America* **79**, 1941–1955.

CAGNIARD, L. 1939. *Réflection et Réfraction des Ondes Séismiques Progressives.* Gauthiers-Villars, Paris, France.

CAGNIARD, L. 1962. *Reflection and Refraction of Progressive Seismic Waves*, translated from French by E. A. Flinn and C. H. Dix. McGraw-Hill Book Co.

ČERVENÝ V. and RAVINDRA, R. 1971. *Theory of Seismic Head Waves.* University of Toronto, Toronto, Canada.

CHAPMAN, C.H. and DRUMMOND, R. 1982. Body-wave seismograms in inhomogeneous media using Maslov asymptotic theory. *Bulletin of the Seismological Society of America* **72**, S277–S317.

CHAPMAN, C.H. and ORCUTT, J.A. 1985. The computation of body wave synthetic seismograms in laterally homogeneous media. *Reviews of Geophysics* **23**, 105–163.

CHOUDHARY, S. and FELSEN, L.B. 1973. Asymptotic theory for inhomogeneous waves. *IEEE Transactions on Antennas and Propagation* **AP-21**, 827–842.

DALEY, P.F. and HRON, F. 1983. Nongeometric arrivals due to highly concentrated sources adjacent to plane interfaces. *Bulletin of the Seismological Society of America* **73**, 1655–1671.

DE HOOP, A.T. 1960. A modification of Cagniard's method for solving seismic pulse problems. *Applied Scientific Research* **B8**, 349–356.

DIEBOLD, J.B. 1987. Three-dimensional traveltime equation for dipping layers. *Geophysics* 52, 1492–1500.

DOBRIN, M.B. 1976. *Introduction to Geophysical Prospecting.* McGraw-Hill Book Co.

DRIJKONINGEN, G.G. 1989. On generalized ray theory in inhomogeneous media. Ph.D. thesis, University of Cambridge.

DRIJKONINGEN, G.G. and CHAPMAN, C.H. 1988. Tunneling rays using the Cagniard–De Hoop method. *Bulletin of the Seismological Society of America* **78**, 898–907.

EINZIGER, P.D. and FELSEN, L.B. 1982. Evanescent waves and complex rays. *IEEE Transactions on Antennas and Propagation* **AP-30**, 594–605.

FELSEN, L.B. 1976, Evanescent waves. *Journal of the Optical Society of America* **66**, 751–760.

FUCHS, K. and SCHULZ, K. 1976. Tunneling of low-frequency waves through the subcrustal lithosphere. *Journal of Geophysics* **42**, 175–190.

HELMBERGER, D.V. 1968. The crust–mantle transition in the Bering Sea. *Bulletin of the Seismological Society of America* **58**, 179–214.

HEYMAN, E. and FELSEN, L.B. 1984. Non-dispersive approximation for transient ray fields in an inhomogeneous medium. In *Hybrid Formulation of Wave Propagation and Scattering* L. B. Felsen (ed.), NATO ASI, Series E, **86**, 269–284. Nijhoff.

HEYMAN, E. and FELSEN, L.B. 1987. Real and complex spectra – a generalization of WKBJ seismograms. *Geophysical Journal of the Royal Astronomical Society* **91**, 1087–1126.

HONG, T.-L. and HELMBERGER, D.V. 1977. Generalized ray theory for dipping structure. *Bulletin of the Seismological Society of America* **67**, 994–1008.

HONG, T.-L. and HELMBERGER, D.V. 1978. Glorified optics and wave propagation in nonplanar structure. *Bulletin of the Seismological Society of America* **68**, 1313–1330.

HRON, F. and MIKHAILENKO, B.G. 1981. Numerical modeling of nongeometrical effects by the Alekseev-Mikhailenko method. *Bulletin of the Seismological Society of America* **71**, 1011–1029.

HUDSON, J.A. 1963. SH waves in a wedged-shaped medium. *Geophysical Journal of the Royal Astronomical Society* **7**, 517–541.

KEAREY, P. and BROOKS, M. 1984. *An Introduction to Geophysical Exploration.* Blackwell Scientific Publications.

KELLER, J.B. 1958. *Calculus of Variations and its Applications.* Proceedings of Symposia in Applied Mathematics. **8**, 27–52, L. M. Graves (ed.). McGraw-Hill Book Co.

MELLMAN, G.R. and HELMBERGER, D.V. 1974. High-frequency attenuation by a thin high-velocity layer. *Bulletin of the Seismological Society of America* **64**, 1383–1388.

PAO, Y.H., ZIEGLER, F. and WANG, Y.S. 1989. Acoustic waves generated by a point source in a sloping fluid layer. *Journal of the Acoustical Society of America* **85**, 1414–1426.

STEPHEN, R.A. and BOLMER, S.T. 1985. The direct wave root in marine seismology. *Bulletin of the Seismological Society of America* **75**, 57–67.